Heliyon 10 (2024) e33629

Contents lists available at ScienceDirect

Heliyon

journal homepage: www.cell.com/heliyon

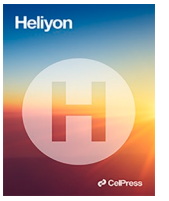

Research article

Self-assembling peptides induced by eyes absent enzyme to boost the efficacy of doxorubicin therapy in drug-resistant breast cancer cells

Emily Carney [a], Forough Ghasem Zadeh Moslabeh [a], Soo-Yeon Kang [b], Bruce A. Bunnell [c], Moo-Yeal Lee [b], Neda Habibi [a,*]

[a] Nanomedicine Lab, Department of Biomedical Engineering, University of North Texas, Texas, United States
[b] Bioprinting Lab, Department of Biomedical Engineering, University of North Texas, Texas, United States
[c] Department of Microbiology, Immunology & Genetics, University of North Texas Health Science Center, Fort Worth, United States

ARTICLE INFO

Keywords:
Peptide
Self-assembly
Enzyme
Breast cancer

ABSTRACT

Enzyme-induced self-assembly (EISA) is a recently developed nanotechnology technique in which small molecules are induced by cellular enzymes self-assembling into nanostructures inside cancer cells. This technique can boost the efficacy of chemotherapy drugs by avoiding drug efflux, inhibiting the cells' DNA repair mechanisms, and targeting the mitochondria. In this work, we study the self-assembly of a short peptide and its fluorescence analogue induced by Eyes absent (EYA) tyrosine phosphatases to boost the efficacy of doxorubicin (DOX) therapy in drug-resistant types of breast cancer cells, MDA-MB-231 and MCF-7. The peptides Fmoc–FF–YP and NBD–FF–YP were synthesized with the solid-phase peptide synthesis (SPPS) method and analyzed with HPLC and MALDI-TOF. Dynamic light scattering was used to determine the size distribution of peptides exposed to the EYA enzyme *in vitro*. The presence of EYA enzymes in breast cancer cells was confirmed using the western blotting assay. The intracellular location of the peptide self-assembly was studied by imaging fluorescence NBD-tagged peptides. The efficacy of the peptide alone and with DOX was determined against MCF-7 and MDA-MB-231 using MTT and LIVE-DEAD assays. Nucleus and cytoplasm F-actin (Phalloidin) staining was used to determine cell morphology changes in response to the combination therapy of peptides/DOX. At an optimal concentration, the peptides are not toxic to the cells; however, they boost the efficacy of DOX against drug-resistant breast cancer cells. We used state-of-the-art computer-aided techniques to predict the molecular structure of peptides and their interactions with EYA. This study demonstrates an approach for incorporating non-cytotoxic components into DOX combination therapy, thereby avoiding increased systemic burden or adverse effects.

1. Introduction

Innovative strategies must be used to enhance the effectiveness of chemotherapy drugs while minimizing systemic toxicity to overcome drug resistance in cancer cells [1,2]. Enzyme-induced self-assembly (EISA) involves the development of small peptide molecules that assemble into nanostructures both in the pericellular and intracellular cell environments, triggered by the expression of

* Corresponding author. University of North Texas Discovery Park, 3940 N Elm St, Denton, TX, 76207, United States.
E-mail addresses: emilycarney@my.unt.edu (E. Carney), neda.habibi@unt.edu (N. Habibi).

https://doi.org/10.1016/j.heliyon.2024.e33629
Received 29 January 2024; Received in revised form 24 June 2024; Accepted 24 June 2024
Available online 25 June 2024

diseased local enzymes [3,4]. Enzymes initiate self-assembly by converting a non-self-assembling precursor into a self-assembling molecule via bond cleavage, bond formation, or dephosphorylation [5]. Self-assembled peptides have the potential to overcome drug resistance due to their ability to bypass cell receptors, form self-assembling nanostructures within cells to entrap drugs and prevent drug efflux, and target tumor cells' mitochondria to overcome DNA repair [7–10]. The self-assembly mechanism that is triggered by local tumor enzymatic expression will assist chemotherapy drugs to penetrate and remain inside cells to be effective (Fig. 1) [6–9].

Previous research has mainly focused on the alkaline phosphatase (ALP) family of enzymes, with limited reports on esterase and metalloproteinase-induced self-assembly in diseased cells [7–11]. The expression of tyrosine phosphatases has been well-documented as an indicator of several diseases, including cancer and neurodegenerative diseases [12,13]. However, despite the critical role of PTP in diseases, enzyme-induced self-assembly with PTP and its involvement in drug delivery have not yet been explored. In this work, for the first time, we study the self-assembly of short peptides induced by Eye absent (EYA) tyrosine phosphatase enzyme in drug-resistant breast cancer cells. The objective is to design and synthesize small precursor peptides responsive to EYAs to enhance the efficacy of doxorubicin (DOX) in drug-resistant breast cancer cells without inducing systemic toxicity.

It is well documented that EYA enzymes are overexpressed in Triple-negative breast cancer (TNBC), and subunits of EYA2 and EYA3 are correlated to metastasis [14–16]. Triple-negative breast cancer (TNBC) is a particularly aggressive and drug-resistant form of breast cancer [17]. This type of cancer is characterized by the absence of three receptors – ER [18], PRs [19], and HER2 - crucial for successful hormone and targeted therapies. As a result, conventional treatments for breast cancer have limited efficacy when addressing TNBC [16]. While chemotherapy continues to be a vital aspect of treatment in numerous cases, over 50 % of breast cancer patients do not experience its benefits [20] due to acquired drug resistance during treatment or intrinsic resistance of cancer cells. The potential of peptide self-assembly to combat drug-resistant cancers motivated our investigation into the application of combination therapy for triple-negative breast cancer.

We have previously shown that short peptides with tyrosine phosphate N terminal groups have higher specificity to be induced by EYA than ALP enzymes [21]. In this work, we study the self-assembly of a short peptide and its fluorescence analogue, Fmoc–FF–YP and NBD–FF–YP, induced by Eyes absent (EYA) tyrosine phosphatases to boost the efficacy of DOX therapy in drug-resistant types of breast cancer cells, MDA-MB-231 and MCF-7. The small peptide sequence included 1) a tyrosine phosphate activation group (YP), 2) a self-assembling group (Fmoc-FF), and 3) a fluorescence motif (NBD). The peptides of Fmoc–FF–YP and NBD–FF–YP were synthesized with the solid phase peptide synthesis method (SPPS) [22] and analyzed with MALDI-TOF. Dynamic light scattering (DLS) was used to determine the size distribution of peptides exposed to the EYA enzyme *in vitro*. The presence of EYA enzyme in breast cancer cells was evaluated using the western blotting assay. The location of the peptide self-assembly was studied by imaging Fluorescence NBD-tagged peptides. We evaluated the effect of the peptide/DOX on the cell viability of a drug-resistant breast cancer cell line with EYA

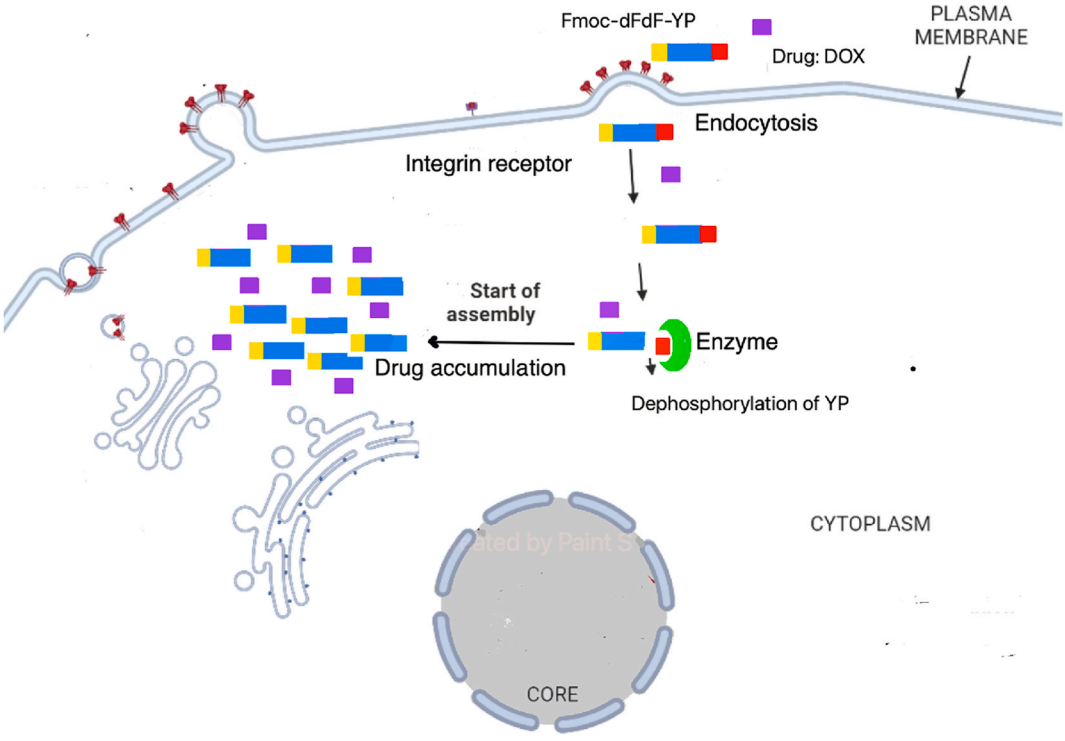

Fig. 1. Peptide self-assembly to nanofibers triggered by enzymes. Peptide sequence: Fmoc–FF–YP. yellow segment: Fmoc, blue segment: FF, red segment: tyrosine phosphate (YP). EYA enzymes dephosphorylate YP and Fmoc-FF will self-assemble into nanofibers.

overexpression, MDA-MB-231 [23], and MCF-7 breast cancer cells. Both breast cancer cell lines are characterized by excessive expression of the EYA enzyme. MDA-MB-231 is TNBC and drug-resistant, and MCF-7 is ER and PR positive, showing resistance to DOX in some cell subtypes. The cells were incubated with the peptide substrates alone and with a combination of the peptides and anti-cancer drugs (DOX). Various techniques such as MTT, LIVE-DEAD, DAPI, and Phalloidin assay were used to determine the drug delivery efficacy with peptides. We leveraged state-of-the-art computer-aided technologies such as I-TASSER [24], PDB, and HADDOCK [25] to predict the molecular 3D structure and interactions of the peptides with the EYA enzyme [24]. The promising results in this research open a paradigm for discovering new therapeutic nano-drugs against drug-resistant breast cancers.

2. Materials and methods

Cell lines, including MCF-7 and MDA-MB-231 breast cancer cells, were purchased from ATCC (USA). Growth mediums and assay kits, including fetal bovine serum (FBS), RPMI, high glucose DMEM, Trypsin-EDTA solution, antibiotics, MTT assay, LIVE-DEAD assay, DAPI staining assay, Phalloidin assay, and green malachite phosphatase assay were all purchased from Thermofisher. EYA enzyme proteins were provided by NOVUS Biologicals (CO, USA).

2.1. Peptide synthesis

In this study, we synthesized and tested two peptide compounds: Fmoc–FF–YP and NBD–FF–YP. The synthesis of peptides followed standard solid phase peptide synthesis (SPPS) protocols using automated peptide synthesizers CSBIO [26]. SPPS is a well-established method used to produce peptides, which short chains of amino acids are linked together by peptide bonds. In SPPS, the peptide chain is built on a solid support, typically a resin. The process begins with the attachment of the first amino acid to the solid support. Then, subsequent amino acids are added one by one, each protected with a temporary blocking group to ensure selective reaction at each step. The widely established Fmoc/*t*Bu approach was utilized, wherein a resin was used as a support. The first amino acid was anchored to the resin via its C-terminal end, employing temporary protecting groups such as *t*Bu (*tert*-butyl) group to protect the side chains of amino acids on the reactive side chain and the alpha-amino group. Subsequent protected amino acids were sequentially added using the coupling approach, progressing through cycles until the peptide sequence was fully synthesized. Once the peptide chain assembly is complete, the peptide is cleaved from the resin and the *t*Bu protecting groups are simultaneously removed. Qualification and quantification of the peptide product were done according to Refs. [21,27,28] and involved MALDI-TOF-MS (Voyager-DE STR Biospectrometry) to identify the accurate mass of peptides and analytical HPLC analysis (Shimadzu Liquid Chromatography system) to identify the purity of peptides. Purification was performed through preparative HPLC based on the desired specifications.

2.2. In-vitro peptide self-assembly, dynamic light scattering, and phosphorylation assay with human EYA enzyme

The in-vitro self-assembly occurs when the precursor peptides are exposed to the EYA enzymes and self-assemble into nanofibers. To explore the self-assembly capability of the peptide, P1 and P2 were initially dissolved in HFP at 100 mg/ml, and this solution was then diluted to a concentration of 2 mg/ml in PBS buffer [29,30]. The EYA enzyme was added at a concentration of 2 U/ml to the peptide solution to induce the in-vitro self-assembly, which was performed using various peptide concentrations ranging from 5 μM) to 100 μM. Dynamic light scattering (DLS) analysis was conducted using a Malvern ZetaSizer ZS, which measured the size distribution of nanofibers. For SEM analysis, we used an FEI Quanta 200 ESEM. An optical image of the self-assembly process following enzyme incubation was captured using an Olympus inverted microscope IX73 [31].

2.3. Western blotting assay

Western blotting assay was used to confirm the presence of EYA enzymes in breast cancer cells. Initially, both cell lines underwent lysis using a RIPA buffer to extract proteins, which were stored at −80 °C until needed. SDS-PAGE gel electrophoresis was conducted with the protein samples utilizing the Bolt Mini Gel Tank from Life Technologies and 10 cm Bolt Bis-Tris Plus 4–12 % gels and MES running buffer. Sample preparation adhered to the user manual guidelines, and electrophoresis ensued at 200V, 160 mA starting current, and a run time of 20 min. The Plus2 Pre-stained Protein Standard from Invitrogen was introduced into a separate well for comparative purposes. Following SDS-PAGE, the gel underwent transfer onto a nitrocellulose membrane utilizing the iBlot 2 machine and iBlot2 stacks from Invitrogen, following the provided user manual instructions. The subsequent step involved the execution of Western Blot using the iBind machine from Invitrogen. EYA Rabbit PolyAb was the primary antibody, while HRP-conjugated anti-Rabbit lgG (H + L) functioned as the secondary antibody. Pierce 1-Step Ultra TMB Blotting Solution was applied to the membrane after incubation to visualize the antibody binding bands.

2.4. Fluorescence imaging of NBD-tagged peptides

To directly confirm the location of peptide nanostructures and examine the cellular distribution of the nanostructures in TNBC, we attached proper fluorescent groups to the potent substrates, and used fluorescent microscopy to image the fluorescence-labeled self-assembled peptide nanostructures in the live cells. A fluorophore (4-nitro-2, 1,1-benzoxadiazole (NBD) was used for imaging purposes. Fmoc was replaced with NBD to introduce fluorophore and maintain self-assembly capability. Both cell cultures were incubated with NBD–FF–YP (500 μM), and after 48 h of incubation, the green fluorescence emission was evaluated with a Keyence microscope.

2.5. Breast cancer cell culture and MTT proliferation/viability test

The MDA-MB-231 and MCF-7 human breast cancer cell lines were acquired from ATCC and cultured in DMEM and RPMI-1640 growth medium, respectively. Each growth medium was supplemented with 1 % antibiotics (penicillin and streptomycin) and 10 % fetal bovine serum (FBS). The cells were maintained at 37 °C in a humidified atmosphere containing 5 % CO_2. The culture medium was refreshed every 2–3 days, and cell passaging was performed using a 0.25 % trypsin-EDTA solution when the cells reached 80–90 % confluency. The trypan blue exclusion method was employed to assess cell viability. In this procedure, the cells were harvested and mixed with trypan blue dye at a 1:1 ratio. The stained cells were then counted using a hemocytometer, and the percentage of viable cells was calculated by subtracting the number of stained cells from the total cell count and dividing by the total number of cells. Live cell counting was also conducted using a cell counter, specifically the Countess III system.

To evaluate cell proliferation and viability, the cells underwent an MTT 3-[4,5-dimethylthiazol- 2-yl]-2,5 diphenyl tetrazolium bromide) assay. Initially, the cells were seeded in 96-well plates with a density of 6×10^5 cells per well and were allowed to adhere overnight. Subsequently, the cells were treated with different concentrations of the peptide compounds, namely 1: Fmoc–FF–YP, 2: NBD–FF–YP, peptide/DOX combinations, and control groups for 48 h. Following the treatment period, the medium was replaced with fresh medium containing MTT solution at a concentration of 0.5 mg/ml, and the cells were incubated for 4 h at 37 °C. The resulting formazan crystals were then dissolved in DMSO, and the absorbance was measured at 570 nm using a microplate reader [32]. All experiments were conducted in triplicate, and the data are presented as the mean ± standard deviation (SD). Statistical analysis was conducted using the *t*-test method for comparing means between two groups. P value less than 0.05 is considered significant.

2.6. Cell viability using LIVE-DEAD assay

The LIVE-DEAD assay was utilized for both MDA-MB-231 and MCF-7 to evaluate the viability of the breast cancer cells. The cells were cultured in RPMI 1640 medium and DMEM supplemented with 10 % fetal bovine serum and 1 % penicillin/streptomycin. The cell cultures were maintained at 37 °C in a humidified atmosphere with 5 % CO_2. Upon reaching approximately 80 % confluency, the cells were detached using trypsin-EDTA and seeded in a 96-well plate at a density of 1×10^4 cells per well.

The LIVE-DEAD assay was performed utilizing the LIVE/DEAD Viability/Cytotoxicity Kit, following the protocol provided by the manufacturer. In brief, the cells were incubated with a mixture of calcein-AM and ethidium homodimer-1 for 30 min at room temperature. Subsequently, the cells were imaged using a fluorescence microscope. The green fluorescence of calcein-AM indicated live cells, while the red fluorescence emitted by ethidium homodimer-1 indicated dead cells. To quantify and visualize the fluorescence signals indicative of live and dead cells, we utilized a microplate reader equipped with green and red filter cubes. These filter cubes selectively excite fluorophores emitting in the green and red spectral ranges, respectively, enabling precise measurement of fluorescence intensity. By recording the green fluorescence emissions of each well, we generated quantitative data reflecting the relative abundance of live cells across the sample population. Subsequently, these data were processed, compared to control samples and plotted to graph to indicate viability percentage. All experiments were carried out in triplicate to ensure the reliability and consistency of results [33].

2.7. Phalloidin assay for staining cytoplasm F-actin and DAPI assay for staining cell nucleus

To investigate the effects of the peptide compounds, the cells were treated for 24 h. When the cells reached an approximate confluency of 80 %, they were fixed using 4 % paraformaldehyde for 15 min. Subsequently, permeabilization was achieved by treating the cells with 0.1 % Triton X-100 for 10 min at room temperature. A thorough washing step with phosphate-buffered saline (PBS) followed, and then the cells were blocked with 1 % bovine serum albumin (BSA) in PBS for 1 h at room temperature.

To visualize the nuclei, the cells were stained with 4',6-diamidino-2-phenylindole (DAPI), and for the F-actin cytoskeleton, Phalloidin staining was employed. The staining procedure was conducted according to the instructions provided by the manufacturer. The cells were incubated with DAPI and Phalloidin for 30 min at room temperature and washed with PBS to remove excess staining. The stained cells were then imaged using a fluorescence microscope to observe the cellular structures. All experiments were meticulously conducted in triplicate to ensure the accuracy and reliability of the results.

3. Results & discussion

We have been exploring the self-assembly of peptides induced by local diseased enzymes in cells. Our earlier research demonstrated that peptides based on diphenylalanine, namely Phe-Phe and Fmoc-Phe-Phe, possess exceptional self-assembling ability and can serve as hydrogelator precursors [21,22,29]. This phenomenon can be attributed to the robust intermolecular π-π interactions occurring in the aromatic rings present in the peptides. While Fmoc-FF ultra-short peptides have great self-assembly without enzymatic assistance, introduction of YP at the C-terminal end in the peptide Fmoc–FF–YP alters its self-assembling behavior. This modification enhances the peptide's solubility, thereby decreasing its self-assembling capability without an enzymatic trigger. In our recent results, we showed that including a phosphotyrosine group (YP) in the end terminal of Fmoc-FF peptide will alter self-assembling behavior and increase selective targeting to be induced by EYAs compared to alkaline phosphatase and allow for enzymatic hydrogelation [21]. EYA enzymes, initially found in embryonic stages, undergo reactivation and expression in different cancers, including breast cancer. The remarkable specificity and novel mechanisms exhibited by molecular nanofibers in targeting cancer cells have motivated us to investigate the potential of peptide-based molecular self-assembly for the multimodal therapy of DOX in drug-resistant breast cancer

cells.

This study determined the combination therapy of D-peptides enantiomer of FF-based peptides with DOX anticancer drugs in different breast cancer cells. TNBCs are often treated with genotoxic chemotherapies such as DOX and cisplatin. However, these genotoxic therapies often promote DNA repair through H2AX signaling with consequent facilitation of cell survival and the development of drug resistance [28]. TNBC cells such as MDA-MB-231 show resistance to DOX therapy [29]. Self-assembly of peptides responsive to breast cancer enzymatic activity could potentially avoid DNA repair and increase cell apoptosis. We synthesized two D-peptide compounds using the solid phase peptide synthesis approach (SPPS): P1: Fmoc-*d*-Phe-*d*-Phe-tyrosine phosphate (Fmoc-dFdF-YP), P2: Nitrobenzofurazan-*d*-Phe-*d*-Phe-tyrosine phosphate (NBD-dFdF-YP). NBD is a fluorescence motif that will allow imaging of the peptide intracellular uptake in cells, and Fmoc-FF is a motif with self-assembling capability. In our research, we opted for the D enantiomer precursor peptides as they exhibited greater proteolytic stability of the nanofibers both extracellularly and intracellularly [30]. During the SPPS approach, initially, phenylalanine (Fmoc-Phe-OH) is loaded onto a solid support. This is followed by SPPS, which results in the creation of Fmoc-FF [16]. Tyrosine phosphate is then coupled with Fmoc-FF [16]. In the P2 compound, tyrosine phosphate is coupled to NBD-FF to achieve P2. Upon purification through HPLC, the yield of P-1 is roughly 90 % and the yield of P2 is about 80 %. MALDI-TOF graphs confirmed a molecular weight of 777 g/mol and 800 g/mol for Fmoc–FF–YP and NBD–FF–YP (Supplement file).

Additionally, our objective was to explore how cellular internalization influences the efficacy of the combined treatment approach. First, we evaluated the in-vitro enzymatic activity of EYA in catalyzing phosphorylation of P1 and P2, resulting in hydrogelation and nanofiber formation. The addition of P1 and P2 in PBS at pH 7.4 with the enzyme and samples were tested at different time points of 10, 30, and 60 min. The samples were put on silicone and SEM was used to visualize the nanofiber. SEM images showed that EYA can convert both P1 and P2 into nanofibers (Fig. 2A). The minimum gelation concentrations for P1 and P2 were 10 and 5 μM, which shows the capability of these compounds to form hydrogels even at low concentrations. After confirming that EYA converts P1 and P2 into nanofibers, we determined the size range of peptide particles using DLS to help confirm the existence of nanostructures in the solution at different concentrations (5–50 μM). After exposure of P1 with EYA, samples were collected and analyzed with Zetasizer (Fig. 2B). The DLS size distribution graphs showed that at 5 μM, there is a low increase of intensity ratio, confirming the offset of self-assembly. The size of particles and intensity increased with concentration, especially with concentrations above 50 μM. The intensity ratio of peptides alone (100 μM) without EYA enzyme indicated a low value, confirming very few self-assembled structures. This confirms that Fmoc–FF–YP peptide have little self-assembly before getting induced by enzymes. Additionally, our visual observations shows that Fmoc-FF develops a stiff gel, however Fmoc–FF–YP does not develop a gel without enzymes. The results of our study demonstrated that the EYA enzyme can transform P1 and P2 into their respective self-assembling molecules, which can form nanofibers in aqueous solutions.

The size distribution measured by DLS results gives insights into the peptides' critical aggregation concentrations (CAC). For self-assembled peptides, the CAC represents the concentration at which these peptides start forming aggregated assembled structures. Studying the CAC would be important to predict appropriate dosing of peptides to ensure high efficacy of self-assembly within the cells. The activating and self-assembling groups are the main segments that determine the self-assembly kinetics and specificity against the enzymes. In the design of peptides, the self-assembled segments can vary from having low to high micelle concentrations. Based on

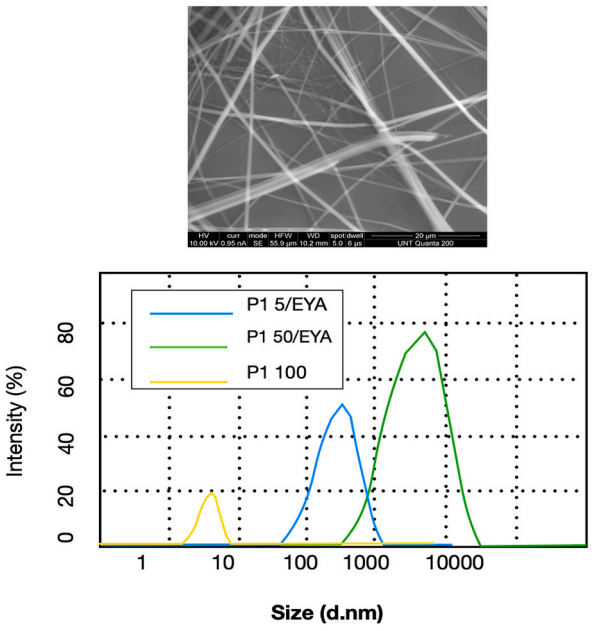

Fig. 2. A: SEM image of Fmoc–FF–YP after exposure to EYA enzyme (50 μM), B: Dynamic Light Scattering displays the size of P1 nanostructures.

existing literature [27] and our own investigative findings, we predict that at a low micelle concentration, the system may remain stable before reaching the disease site but may not produce enough micelles to form stable structures at the disease site. The system has densely packed micelles at a high micelle concentration, leading to more stable structures for drug delivery. However, the drawback is that the system may produce micelles before reaching the disease site. The goal is to determine the suitable self-assembling segment that produces enough micelles at the site but remains stable before reaching the site. The critical micelle concentration obtained in this research will give important insight for choosing a suitable design and concentration that will lead to this goal. In-vitro phosphatase assays indicated that phosphorylation starts in the first 10 min of enzyme exposure and reaches a stable value after 2 h.

We used the I-TASSER protein analysis database to predict the structure of Fmoc–FF–YP. The database predicts the solvent accessibility of residues, normalized B-factor indicating the mobility of residues in the peptide, and the top 5 likely models of the peptide 3D structure. Both ends of the peptides are predicted to be coiled with a normalized B-factor of 2, and the FF segment is stranded with a normalized B-factor of 1. The B-factor indicates the average displacement of atoms from their equilibrium positions. High B-factor values suggest greater atomic motion or disorder, while low values indicate less motion or greater precision in the determined positions. The ligand binding site predicted by HADDOCK suggests residues 4 and 5 of the peptide will have the highest C-score (confidence prediction score) to interact with the tyrosine phosphatase active site of EYA (Fig. 3).

NBD-tagged peptides were used to directly confirm the location of peptide nanostructures and examine the cellular distribution of the nanostructures in TNBC. Both cells were incubated with P2: NBD–FF–YP (500 μM), and after 24 and 72 h, the fluorescence emission was detected (Fig. 4 A, B). The results indicated a strong green fluorescence emerging from the region inside the cells (Fig. 4A and B), suggesting that the self-assembly of P2 is intracellular and results in the formation of the nanofibers detectable with the microscope. The fluorescence emission for both cell lines were increased at 72 h indicating that the self-assembly is enhanced by time. Western blot assays were performed to confirm the presence of EYA enzymes in breast cancer cells. The full-length stained Western blot membranes are shown in Fig. 4C. The binding assay utilized EYA3 Rabbit PolyAb as the primary antibody and HRP-conjugated anti-Rabbit lgG (H + L) as the secondary Abs. After staining the membrane, the EYA band was identified in both cancer cells, in which MCF-7 showed a thicker band, indicating a higher amount of EYA enzymes. Notably, the fluorescence emission of NBD-tagged peptides was also higher in MCF-7 cells, indicating a correlation between EYA expression and peptide self-assembly. Proteointech reports that the EYA enzyme comprises three isoforms with molecular weights of 50–59 kDa, which is consistent with the molecular weight of EYA identified in our study.

To assess the influence of P1 and P2 self-assembly on the efficacy of DOX-based therapy, we performed MTT cell viability assays on two distinct breast cancer cell lines. Firstly, we used MDA-MB-231, which is a triple-negative breast cancer cell line that is known to express EYA enzyme and shows resistance to DOX therapy. Secondly, we used MCF-7, which is an ER, PR-positive breast cancer cell line that shows dysregulation expression of EYA and, in some cases, resistance to DOX therapy. These tests involved incubating the cell

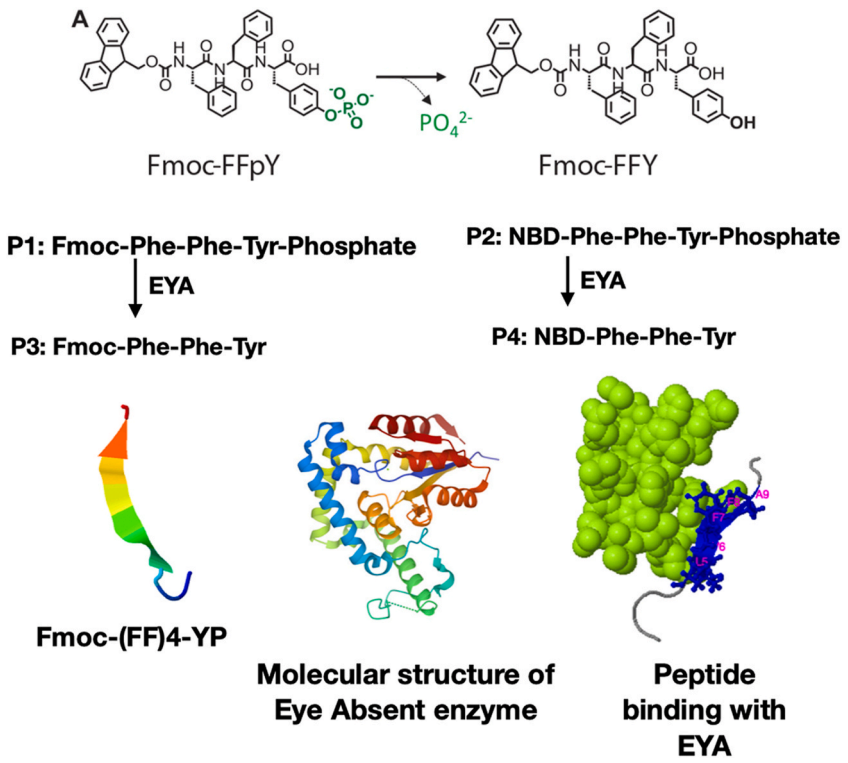

Fig. 3. Peptide precursor sequence design, molecular 2D drawn with Marvin Sketch and 3D structures prediction with I-TESSAR, and interaction with EYA enzymes predicted with HADDOCK.

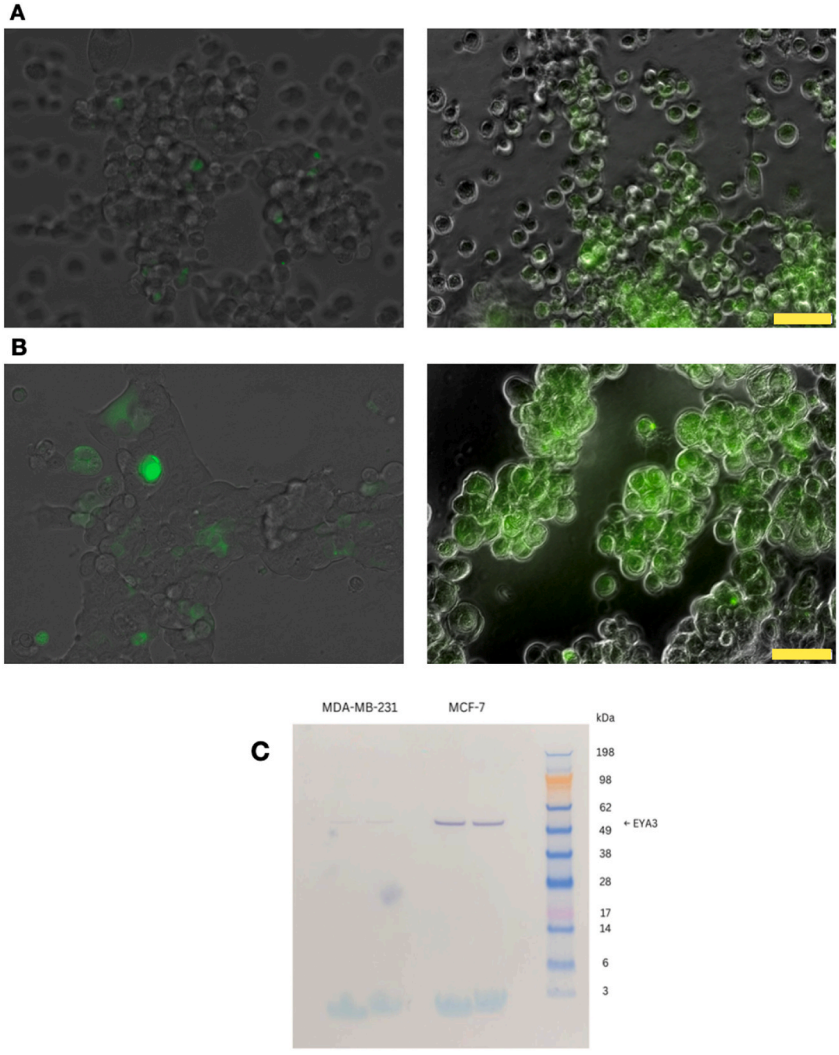

Fig. 4. Fluorescence image of peptide self-assembly in A) MDA-MB-231, and B) MCF-7, breast cancer cells incubated with 500 μM NBD–FF–YP peptides after 24 h (left), and 72 h (right). Exposure time is 1 s. The green emission confirms the location of NBD–FF–YP peptide self-assembly in the cell culture. Scale bar is 50 μM. C: Full-length Western blot image analysis of EYA3 enzymes in breast cancer cells.

lines with a combination of precursors and DOX.

Fig. 5A and B shows the viability of both cell lines after 48 h of exposure with a combination of DOX (30 μg/ml) with P1 and P2 at concentrations of 10–500 μM. After 48 h of exposure, DOX alone inhibited 35 % of MDA-MB-231 cells (Fig. 5A). The P1 precursor, when used at concentrations between 10 and 500 μM alone, inhibited 25–35 % of cells. However, when DOX was combined with P1 at concentrations ranging from 50 to 500 μM, it inhibited 72–80 % of cells and increased the efficacy of DOX alone twofold. When the P2 compound was used alone, at 10–500 μM concentrations, it inhibited 20–50 % of cells. The combination of DOX/P2, 10–500 μM, inhibits 70 % of cells, which enhances the activity of DOX alone two-fold. The combined application of P1, P2, and DOX has been found to suppress MDA-MB-231 cells significantly and reduce their viability from 65 % (without P1 or P2) to 20–30 %. In MCF-7 cells, after 48 h of treatment, DOX alone inhibits 24 % of the cells (Fig. 5B). The combination therapy of DOX/P1, P2, 10–500 μM inhibited 45–50 % of the cells, which enhances the effect of DOX alone twofold.

The MDA-MB-231 cell line is known for its drug resistance in breast cancer, demonstrated by lower inhibition by DOX than other cell lines. Incorporating precursors of self-assembling small molecules into the DOX-based combination therapy greatly enhanced DOX's activity against drug-resistant breast cancer cells. These findings suggest that the DOX/P2, P1 combination therapy holds immense potential in inhibiting drug-resistant cells, with the peptides exhibiting relatively low toxicity to the cells. The IC50 values of P1 and P2 alone against MDA-MB-231 are 500 μM, but their concentrations can be as low as 10 μM for combination therapy. We suggest that this approach enables intracellular accumulation of hydrogelators with the drugs.

To provide direct visualization of live and dead cells and to identify the location of dead cells within a heterogeneous population, we used the LIVE-DEAD assay (Fig. 6A). Cells were treated with P1 and P2 (10 and 100 μM) and stained with calcein-AM and ethidium

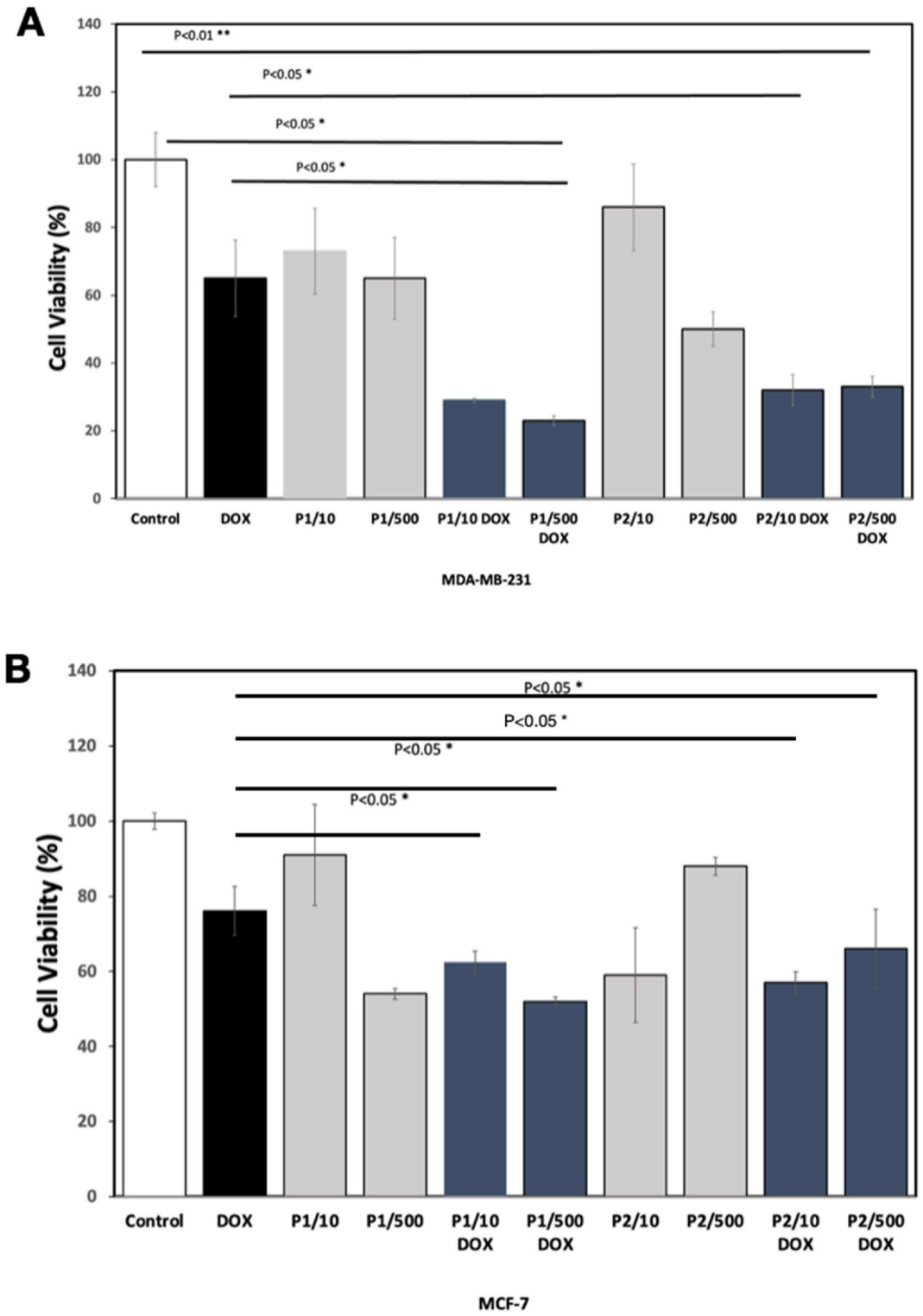

Fig. 5. MTT viability cell assay of A: MDA-MB-231 cells and B: MCF-7 cells with P1, P2 and a combination of P1/DOX and P2/DOX after 48 h exposure to peptides. P value less than 0.05 is considered significant.

homodimer-1. Live cells are visualized as green fluorescence upon staining with calcein-AM dye, while dead cells exhibit red staining when treated with ethidium homodimer-1 dye. Fluorescence microscopy was utilized to observe the cell cultures, and the fluorescence emission was quantified using a microplate spectrometer (Fig. 6B). The images were also analyzed with Image J software. As shown clearly in Fig. 6A, combining P1 and P2 with DOX significantly increased the number of red dead cells compared to DOX alone. P2/DOX 100 μM increased the activity of DOX alone three-fold, and P1/DOX 100 μM alone reduced the viability from 52 % to 40 % compared to DOX alone. The viability of MCF-7 cells treated with DOX alone was 80 %, which was decreased to 45 % and 58 % with a combination of P1/DOX and P2/DOX, respectively (Fig. 6B).

To explore the impact of peptide self-assembly, we examined the alterations in actin filaments within the cellular environment. Fig. 7 shows that treatment of MDA-MB-231 cells with P-1 at a concentration of 10 μM for 24 h resulted in less well-defined and elongated actin filaments compared to the control cells which were untreated with P-1 (Fig. 7). This effect was more prominent at a higher concentration of 100 μM, as seen by the decreased amount of actin filaments within the cells. These findings suggest that small peptide intracellular nanofibers can interact with actins, supporting decreased actin filament formation. It is worth noting that the cells exposed to both the peptide and DOX exhibited a remarkable transformation. Only a few viable cells were observed, and the F-actin structure underwent complete deformation. To gain insights into the reversibility of F-actin-induced changes, we treated cells with P1 at concentrations of 10 and 100 μM for 24 h and subsequently replaced the peptide with fresh medium and treated for an extra 20 h. The findings demonstrated the restoration of actin filaments following the treatment with fresh medium, however, at a concentration of 100 μM, incomplete recovery was observed, suggesting a threshold of irreversible cell changes at higher concentrations. We suggest that the formation of nanofibers through self-assembly demonstrates temporary cytotoxicity, which may contribute to reducing long-term systemic side effects in combination therapy. Degradation of the nanofibers to a high extent decreases long-term cytotoxicity after apoptosis of cells, minimizing systemic toxicity caused by precursors and nanofibers.

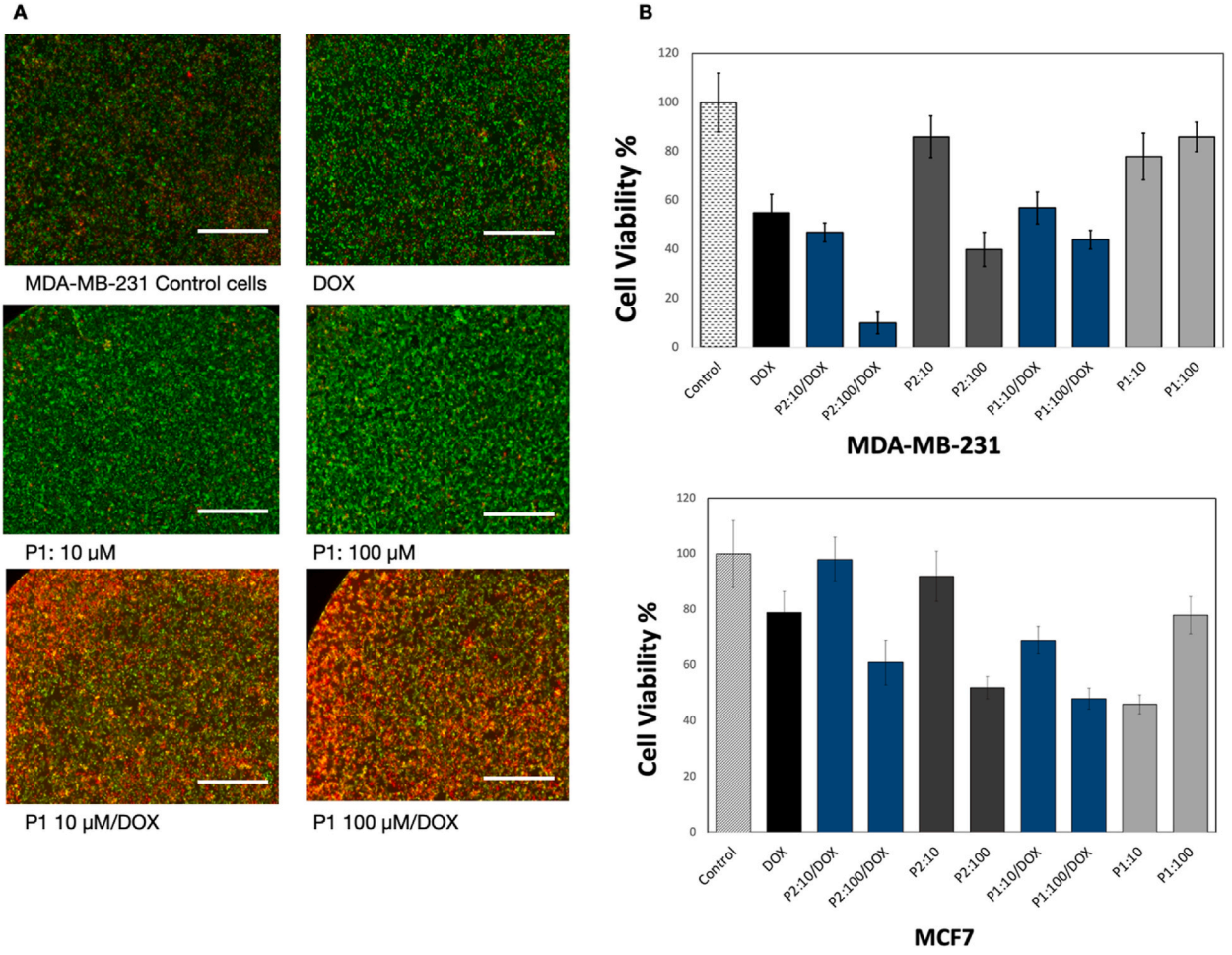

Fig. 6. A: Fluorescence image of LIVE-DEAD cell assay (Live cells convert calcein AM to green, fluorescent calcein, while dead cells are stained with red fluorescent ethidium homodimer-1. B: Cell viability analyzed with live-dead assay of MDA-MB-231 cells and MCF-7 cells with P1, P2 and a combination of P1/DOX and P2/DOX. Scale bar is 200 μm.

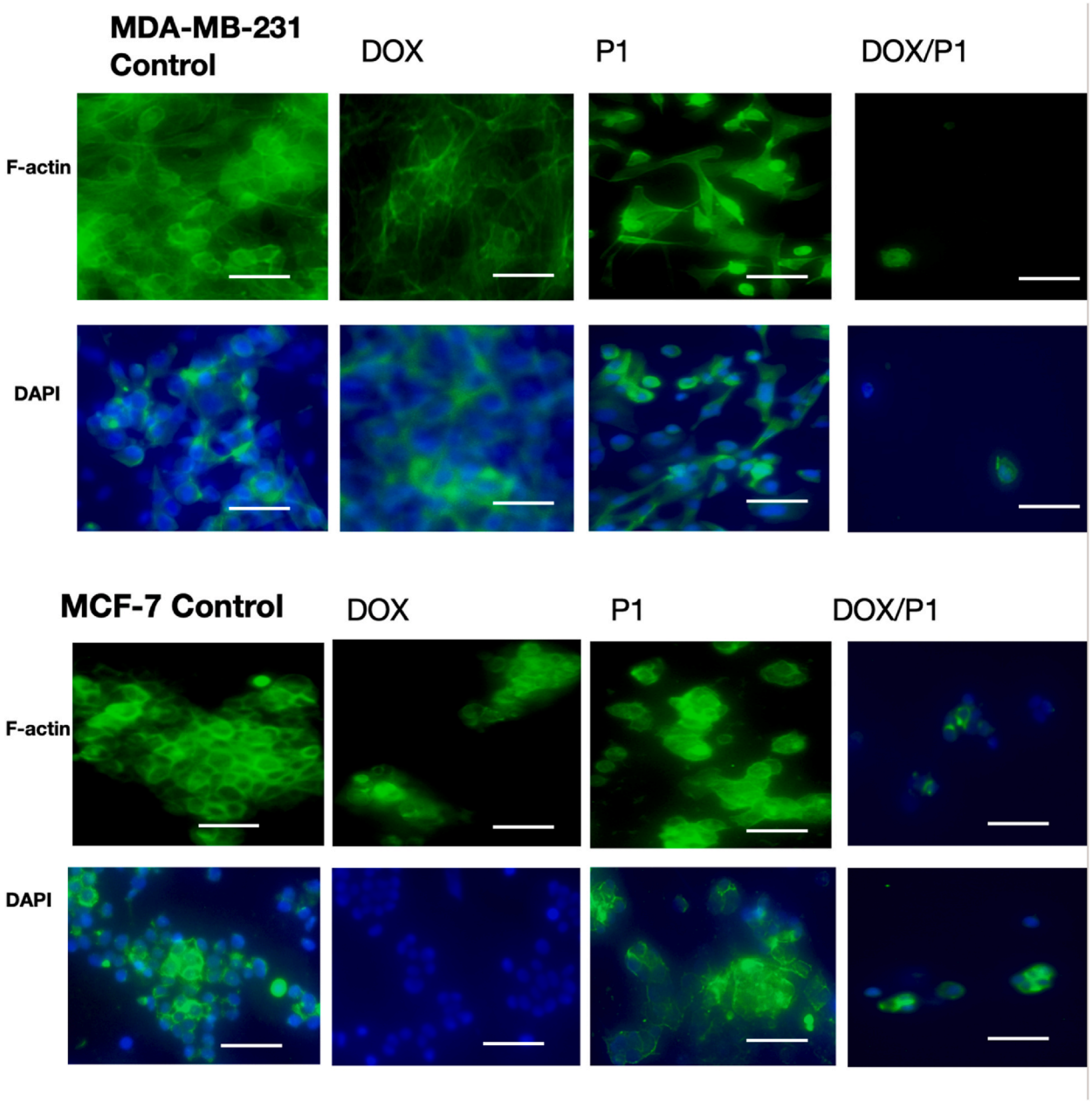

Fig. 7. DAPI (nucleus) and Phalloidin (F-actin) staining of MDA-MB-231 cells with P1 and combination of P1/DOX. The cytoplasm is stained green, and the nucleus is stained blue. Scale bar is 50 μm.

4. Conclusions

This study demonstrated the feasibility of combining two peptide precursors with DOX in treating drug-resistant breast cancer cells. We synthesized P1 and P2 with the structure of Fmoc–FF–YP and NBD–FF–YP. We suggest that the tyrosine phosphatase activity of EYA can convert the precursor to self-assembling molecules inside the cells. In this work, for the first time we show the potential link between tyrosine phosphatase enzymes (EYA) and the self-assembly of ultra-short peptides, elucidating their impact on drug resistance in breast cancer cells. Initially, we confirmed the presence of EYA enzymes in drug-resistant breast cancer cells. Subsequently, we demonstrated the intracellular uptake of peptides and the progressive self-assembly within the cells over time. Furthermore, we conducted various cell-based assays including MTT, LIVE-DEAD, Phalloidin cytoplasm staining, and analysis of DNA morphology. These assays collectively affirmed the peptides' efficacy in enhancing the effectiveness of DOX therapy. This consistent data strongly suggests that peptides substantially boost the therapeutic efficacy of DOX, presenting a promising avenue in drug discovery that holds

potential benefits for researchers. This study and additional evidence of enzyme-induced self-assembly [34,35] highlight the potential of modified peptides as a promising novel approach for selectively targeting TNBC. For future work, we aim to investigate the mechanism of death pathways by analyzing mitochondria, membrane, and DNA damage [36–38]. By investigating the H2AX DNA repair pathways, we can get insights into the effect of peptides on DNA repair signaling [39–42].

CRediT authorship contribution statement

Emily Carney: Resources, Methodology, Investigation, Formal analysis. **Forough Ghasem Zadeh Moslabeh:** Methodology. **Soo-Yeon Kang:** Resources, Methodology. **Bruce A. Bunnell:** Writing – review & editing, Supervision. **Moo-Yeal Lee:** Supervision, Resources. **Neda Habibi:** Writing – original draft, Supervision, Methodology, Conceptualization.

Declaration of competing interest

The authors declare that they have no known competing financial interests or personal relationships that could have appeared to influence the work reported in this paper.

Acknowledgment

Research reported in this publication was supported by the National Institute of General Medical Science (NIGMS) of the National Institutes of Health (NIH), United States, under award number R16GM150848.

Appendix A. Supplementary data

Supplementary data to this article can be found online at https://doi.org/10.1016/j.heliyon.2024.e33629.

References

[1] H. Wang, Z. Feng, Y. Wang, R. Zhou, Z. Yang, B. Xu, Integrating enzymatic self-assembly and mitochondria targeting for selectively killing cancer cells without acquired drug resistance, J. Am. Chem. Soc. 138 (49) (2016) 16046–16055. - PMID: 27960313.
[2] P. Khosravi-Shahi, L. Cabez′on-Guti′errez, S. Custodio-Cabello, Metastatic triple-negative breast cancer: optimizing treatment options, new and emerging targeted therapies, Asia Pac. J. Clin. Oncol. 14 (1) (2018) 32–39.
[3] J. Li, J. Shi, J.E. Medina, J. Zhou, X. Du, H. Wang, et al., Selectively inducing cancer cell death by intracellular enzyme-instructed self-assembly (EISA) of dipeptide derivatives, Adv. Healthcare Mater. 6 (15) (2017) 1601400.
[4] Z. Feng, H. Wang, X. Chen, B. Xu, Self-assembling ability determines the activity of enzyme-instructed self-assembly for inhibiting cancer cells, J. Am. Chem. Soc. 139 (43) (2017) 15377–15384.
[5] X. Li, Y. Wang, Y. Zhang, Z. Yang, J. Gao, Y. Shi, Enzyme-instructed self-assembly (EISA) assists the self-assembly and hydrogelation of hydrophobic peptides, J. Mater. Chem. B 10 (17) (2022) 3242–3247.
[6] J. Gao, J. Zhan, Z. Yang, Enzyme-instructed self-assembly (EISA) and hydrogelation of peptides, Adv. Mater. 32 (3) (2020) 1805798.
[7] J. Zhou, B. Xu, Enzyme-instructed self-assembly: a multistep process for potential cancer therapy, Bioconjugate Chem. 26 (6) (2015) 987–999.
[8] J. Li, Y. Kuang, J. Shi, J. Zhou, J.E. Medina, R. Zhou, et al., Enzyme-instructed intracellular molecular self-assembly to boost the activity of cisplatin against drug-resistant ovarian cancer cells, Angew. Chem. Int. Ed. 54 (45) (2015) 13307–13311.
[9] Y. Gao, Z. Yang, Y. Kuang, M.L. Ma, J. Li, F. Zhao, et al., Enzyme-instructed self-assembly of peptide derivatives to form nanofibers and hydrogels, Peptide Science: Original Research on Biomolecules 94 (1) (2010) 19–31.
[10] F. Lin, C. Jia, F.G. Wu, Intracellular enzyme-instructed self-assembly of peptides (IEISAP) for biomedical applications, Molecules 27 (19) (2022) 6557.
[11] M. Nedeljkovi′c, A. Damjanovi′c, Mechanisms of chemotherapy resistance in triple-negative breast cancer—how we can rise to the challenge, Cells 8 (9) (2019) 957.
[12] A. Marra, D. Trapani, G. Viale, C. Criscitiello, G. Curigliano, Practical classification of triple-negative breast cancer: intratumoral heterogeneity, mechanisms of drug resistance, and novel therapies, NPJ Breast Cancer 6 (1) (2020) 1–16.
[13] A. Carina Hellberg, F.D. Böhmer, Protein-tyrosine phosphatases and cancer, Nat. Rev. Cancer 6 (2006) 307–320.
[14] H. Zhou, L. Zhang, R.L. Vartuli, H.L. Ford, R. Zhao, The Eya phosphatase: its unique role in cancer, Int. J. Biochem. Cell Biol. 96 (2018) 165–170. -PMID: 28887153.
[15] A.B. Krueger, S.J. Dehdashti, N. Southall, J.J. Marugan, M. Ferrer, X. Li, et al., Identification of a selective small-molecule inhibitor series targeting the eyes absent 2 (Eya2) phosphatase activity, J. Biomol. Screen 18 (1) (2013) 85–96.
[16] R. Vartuli, Eya3 Threonine Phosphatase Promotes Triple Negative Breast Cancer Growth through PD-L1 Regulation of the Tumor Adaptive Immune Response, University of Colorado at Denver, Anschutz Medical Campus, The, 2017.
[17] H. Yao, G. He, S. Yan, C. Chen, L. Song, T.J. Rosol, et al., Triple-negative breast cancer: is there a treatment on the horizon? Oncotarget 8 (1) (2017) 1913.
[18] Y. Sun, S. Kaneko, X. Li, X. Li, The PI3K/Akt signal hyperactivates Eya1 via the SUMOylation pathway, Oncogene 34 (19) (2015) 2527–2537.
[19] C. Denkert, G. Von Minckwitz, J.C. Brase, B.V. Sinn, S. Gade, R. Kronenwett, et al., Tumor-infiltrating lymphocytes and response to neoadjuvant chemotherapy with or without carboplatin in human epi- dermal growth factor receptor 2-positive and triple-negative primary breast cancers, J. Clin. Oncol. 33 (9) (2015) 983–991.
[20] E.A. O'Reilly, L. Gubbins, S. Sharma, R. Tully, M.H.Z. Guang, K. Weiner-Gorzel, et al., The fate of chemoresistance in triple negative breast cancer (TNBC), BBA Clin. 3 (2015) 257–275.
[21] FG Zadeh Moslabeh, S Miar, N Habibi, In vitro self-assembly of a modified diphenylalanine peptide to nanofibers induced by the Eye absent enzyme and alkaline phosphatase and its activity against breast cancer cell proliferation, ACS Appl. Bio Mater. 6 (1) (2023) 164–170.
[22] N. Habibi, N. Kamaly, A. Memic, H. Shafiee, Self-assembled peptide-based nanostructures: smart nanomaterials toward targeted drug delivery, Nano Today 11 (1) (2016) 41–60.
[23] K.J. Chavez, S.V. Garimella, S. Lipkowitz, Triple negative breast cancer cell lines: one tool in the search for better treatment of triple negative breast cancer, Breast Dis. 32 (1–2) (2010) 35.

[24] Y. Zhang, I-TASSER server for protein 3D structure prediction, BMC Bioinf. 9 (2008) 1–8.
[25] S.J. De Vries, M. Van Dijk, A.M. Bonvin, The HADDOCK web server for data-driven biomolecular docking, Nat. Protoc. 5 (5) (2010) 883–897.
[26] M. Stawikowski, G.B. Fields, Introduction to peptide synthesis, Current protocols in protein science 69 (1) (2012) 18, 1.
[27] Y. Hong, L.S. Lau, R.L. Legge, P. Chen, Critical self-assembly concentration of an ionic-complementary peptide EAK16, J. Adhes. (80) (2004) 913–931.
[28] C.T. Mant, Y. Chen, Z. Yan, T.V. Popa, J.M. Kovacs, J.B. Mills, et al., HPLC analysis and purification of peptides, in: Peptide Characterization and Application Protocols, Springer, 2007, pp. 3–55.
[29] S. Yazdani, S.M. Ghoreishi, N. Habibi, Effects of Co-solvents on loading and release properties of self-assembled di-peptide building blocks, towards drug delivery applications, Protein Pept. Lett. 29 (1) (2022) 80–88.
[30] T. Zohrabi, N. Habibi, A. Zarrabi, M. Fanaei, L.Y. Lee, Diphenylalanine peptide nanotubes self-assembled on functionalized metal surfaces for potential application in drug-eluting stent, J. Biomed. Mater. Res. 104 (9) (2016) 2280–2290.
[31] J. Li, Y. Gao, Y. Kuang, J. Shi, X. Du, J. Zhou, et al., Dephosphorylation of D-peptide derivatives to form biofunctional, supramolecular nanofibers/hydrogels and their potential applications for intracellular imaging and intratumoral chemotherapy, J. Am. Chem. Soc. 135 (26) (2013) 9907–9914. -PMID: 23742714.
[32] P. Kumar, A. Nagarajan, P.D. Uchil, Analysis of cell viability by the MTT assay, Cold Spring Harb. Protoc. 2018 (6) (2018) pdb–prot095505.
[33] B.A. Pfeffer, S.J. Fliesler, Streamlined duplex live-dead microplate assay for cultured cells, Exp. Eye Res. 161 (2017) 17–29.
[34] G. Emtiazi, T. Zohrabi, L.Y. Lee, N. Habibi, A. Zarrabi, Covalent diphenylalanine peptide nanotube conjugated to folic acid/magnetic nanoparticles for anti-cancer drug delivery, J. Drug Deliv. Sci. Technol. 41 (2017) 90–98.
[35] T. Zohrabi, N. Habibi, Dendritic peptide nanostructures formed from self-assembly of di-L-phenylalanine extracted from Alzheimer's β-amyloid poly peptides: insights into their assembly process, Int. J. Pept. Res. Therapeut. 21 (4) (2015) 423–431.
[36] N. Srivastava, S. Gochhait, P. de Boer, R.N. Bamezai, Role of H2AX in DNA damage response and human cancers, Mutat. Res. Rev. Mutat. Res. 681 (2–3) (2009) 180–188.
[37] J.H. Park, K.P. Kim, J.J. Ko, K.S. Park, PI3K/Akt/mTOR activation by suppression of ELK3 medi- ates chemosensitivity of MDA-MB-231 cells to doxorubicin by inhibiting autophagy, Biochem. Biophys. Res. Commun. 477 (2) (2016) 277–282.
[38] J. Zhou, X. Du, N. Yamagata, B. Xu, Enzyme-instructed self-assembly of small D-peptides as a multiple- step process for selectively killing cancer cells, J. Am. Chem. Soc. 138 (11) (2016) 3813–3823. - PMID: 26966844.
[39] N.A. Dudukovic, C.F. Zukoski, Mechanical properties of self-assembled Fmoc-diphenylalanine molecular gels, Langmuir 30 (15) (2014) 4493–4500.
[40] N.A. Dudukovic, B.C. Hudson, A.K. Paravastu, C.F. Zukoski, Self-assembly pathways and polymorphism in peptide-based nanostructures, Nanoscale 10 (3) (2018) 1508–1516.
[41] M.R. Hajinezhad, S. Shahraki, Z. Nikfarjam, F. Davodabadi, S. Mirinejad, A. Rahdar, S. Sargazi, M. Barani, Development of a new vesicular formulation for delivery of Ifosfamide: evidence from in vitro, in vivo, and in silico experiments, Arab. J. Chem. 16 (9) (2023) 105086.
[42] A. Huang, W. Zhou, Mn-based cGAS-STING activation for tumor therapy, Chin. J. Cancer Res. 35 (1) (2023) 19–43.